Submitted to

International Europhysics Conference on High Energy Physics, July 12, 2001, Budapest

EPS 2001:	Abstract:	**816**
	Parallel Sessions	**1, 2**

XX International Symposium on Lepton and Photon Interactions, July 23, 2001, Rome

LP 2001:	Abstract:	**508**
	Plenary Session	**S8**

www-h1.desy.de/h1/www/publications/conf/conf_list.html

Comparison of Fragmentation Properties in Diffractive and Non-Diffractive Deep-Inelastic scattering at HERA.

H1 Collaboration

Abstract

Fragmentation measurements are presented for diffractive and non-diffractive deep inelastic *ep* scattering data in the Breit frame of reference. The rapidity spectra for the diffractive event selection clearly shows the expected suppression of tracks in the target hemisphere. The average charged multiplicity in the current hemisphere, $< n >$, is shown to compare well with DIS at low β and with e^+e^- at high β. The evolution of the peak and width of the current hemisphere fragmentation functions for charged particles is studied as a function of photon virtuality, Q, and is found to agree with results obtained in non-diffractive deep inelastic scattering. Comparison with various models of diffraction are made with the resolved pomeron model (H1 fit 2) providing the best description of the data.

1 Introduction

Previous studies [1, 2, 3, 4] of Deep Inelastic ep Scattering (DIS) in the Breit frame of reference [5] have established the universality of hadronic fragmentation properties and their energy dependence for quarks ejected from a proton and for quarks produced from the vacuum in e^+e^- annihilation experiments.

There exists a subclass of DIS events of distinctly separate properties, called diffractive events. These events are identified by a gap in rapidity between the observed hadronic system X , and the outgoing proton system Y. These events are evidence of a colourless exchange mechanism between the proton and exchange boson, commonly referred to as pomeron ($I\!\!P$) exchange.

It is a principal object of this paper to further test universal fragmentation by examining the fragmentation properties of quarks thrown out of the pomeron in diffraction when probed with the same highly virtual boson as used in ep DIS scattering.

It is useful to recall some of the variables used in the description of DIS in general and diffraction in particular. The total hadronic energy of the $\gamma^* p$ system is W, the magnitude of the four momentum transfer is Q and $M_{\rm x}$ is the mass of the observed hadronic final state in the central detectors ($\gamma^* I\!\!P$ system). We also define the Lorentz invariant dimensionless variables

$$t = (p - p')^2, \tag{1}$$

$$\beta = \frac{Q^2}{2\,(p - p')\cdot q} \simeq Q^2/(M_{\rm x}^2 + Q^2) \tag{2}$$

and

$$x_{I\!\!P} = \frac{(p - p')\cdot q}{p \cdot q} \simeq (M_{\rm x}^2 + Q^2)/(W^2 + Q^2), \tag{3}$$

where the incoming proton four momentum is p, the outgoing proton momentum is p' and the four momentum of the exchange boson is q. The squared four momentum transferred at the proton vertex is t. The proton mass and momentum transfer t have been neglected in the approximation for β and $x_{I\!\!P}$. In the infinite momentum frame, β is the fraction of momentum of the pomeron carried by the struck quark and $x_{I\!\!P}$ is the fraction of momentum of the initial state proton carried by the pomeron.

Diffractive events are selected on the basis of an observed rapidity gap in the forward region of the detector. Previous studies of diffractive phenomena [6] used selections requiring a laboratory pseudorapidity[1] gap in the range $3.3 < \eta < 7.5$. These requirements impose the approximate constraint $M_Y < 1.6$ GeV, $|t| < 1.0$ GeV^2 , $x_{I\!\!P} < 0.05$ and $3.0 < M_x < 36$ GeV. Within this analysis this is referred to as the DIFF selection. Previous DIS studies [1, 2] excluded diffractive events since they were not generated by DIS Monte-Carlos and could therefore not be corrected for. This required a minimum detected energy flow in the forward region and this selection is referred to as the DIS selection.

A particularly suitable frame of reference in which to study quark fragmentation in ep scattering is the Breit Frame [5].

In this frame and within the naive quark-parton model (QPM) the purely space-like virtual photon has longitudinal momentum $-Q$ and collides elastically and head-on with a quark

[1]Pseudorapidity $\eta = -\ln(\tan(\theta/2))$ where θ is measured with respect to the proton beam direction.

of longitudinal momentum $Q/2$. The struck quark is scattered with an equal but opposite momentum while the proton remnant fragments into the opposite hemisphere. Particles emerging from the interaction are assigned to the current region (and associated with the struck quark) if they have negative longitudinal momenta.

The energy scale for the current region, set by the virtual photon, is given by $Q/2$, and is independent of the nature (diffractive or non-diffractive) of the event. Unlike the hadronic center of mass system in DIS, or the center of mass of system X in DIFF, the Breit frame is not a rest frame.

After a description of the relevant parts of the apparatus (section 2) and a discussion of the treatment of data (section 3), we study the rapidity spectra (section 4), the evolution of the fragmentation function (section 5) and the average charged multiplicity (section 6)

2 The H1 Detector

The H1 detector is described in detail elsewhere [7]. Here, we give only a short description of the components more relevant to this analysis. We employ a right-handed coordinate system with the positive (forward) z axis being in the direction of the incoming proton. Polar angles are measured from this direction.

In the central region of the apparatus momentum measurements of charged particles are provided by two cylindrical and co-axial drift chambers [8] which are supplemented by two z-chambers. In the forward (proton) direction, tracks are measured by the Forward Track Detector [9] (FTD) which consists of three Radial and three Planar drift chamber modules. All these track detectors are inside a uniform 1.15T magnetic field. Track segments from all devices are combined to give efficient detection and momentum measurement with $\delta p/p^2 < 1\%/\mathrm{GeV}$ for most of the angular range used in this analysis, ($10^\circ < \theta < 160^\circ$).

In the polar range $4^\circ < \theta < 154^\circ$, the trackers are surrounded by a fine-grained liquid argon (LAr) sampling calorimeter [10] with lead and steel absorber in the electromagnetic and hadronic sections respectively. A backward scintillating fibre calorimeter (SpaCal [11]) covers the range $153^\circ < \theta < 177.8^\circ$ and provides identification and measurement of the scattered positron. The SPACAL detector also gives time of flight information for the efficient removal of beam related background for triggering purposes.

Forward energy at small angles is observed in the outgoing proton beam direction by the Forward Muon Detector (FMD) and the Proton Remnant Tagger (PRT). The FMD covers the pseudo-rapidity range $1.9 < \eta < 3.7$ directly but is also sensitive to larger η values ($3.5 < \eta < 6.5$) as a result of secondary scattering off beam gas and the beam pipe. The PRT consists of scintillation counters surrounding the beam pipe at $z = 24$m, with an effective sensitivity to energy flow in the range $6 < \eta < 8$.

3 Data Selection and Corrections

The data are taken with 27.5 GeV positrons incident on 820 GeV protons giving an ep centre of mass energy, $\sqrt{s}$, of 300 GeV. The trigger requires the identification of a large electromagnetic energy deposited in the backward direction by the SpaCal detector. The trigger is fully efficient ($> 99\%$) and unbiased in both Q and charged track multiplicity using the selection of low Q events described below. The analysis begins with nearly two million events of which nearly half a million survive basic fiducial cuts. This corresponds to an integrated luminosity of about

$7\,\mathrm{pb}^{-1}$. Event kinematic variables used in this analysis are calculated using only the scattered lepton, which gives both good resolution in the chosen region and explicit freedom from bias on the hadronic system studied. Further cuts are made to ensure energy containment of the scattered positron within the SpaCal.

The events are explicitly selected to have an identified scattered positron with an energy $E_e > 14$ GeV. The polar angle of the scattered quark (θ_q), calculated using four momentum conservation with the scattered lepton and assuming the quark is massless, is required to be $10^\circ < \theta_q < 150^\circ$. This is inside the acceptance of the H1 track detectors and thus minimises corrections at the cost of removing a further $\sim 24\%$ of events.

To reject beam associated background, we demand that there be no veto from the time of flight system and that an event vertex be reconstructed within 35 cm of the nominal vertex position. The dimensionless inelasticity variable, $y = Q^2/xs$, is required to be in the range $0.055 < y < 0.6$ and the sum $\sum_i (E^i - p_z^i)$ over all calorimeter energy deposits is required to be larger than 35 GeV and smaller than 70 GeV. Together, these conditions ensure that contamination from mis-identified photoproduction events is below the 1% level and reduce QED radiative effects.

There is a remaining source of error arising from initial state QED radiation. This leads to an incorrect measurement of Q^2 which affects the boost to the Breit frame. The miscalculation of the boost results in a wrongly determined Breit frame axis. In most cases this leads to a depleted (or even empty) region of phase space where the scattered quark fragments are expected. To reduce the size of the necessary QED corrections, this analysis reimposes the $0.055 < y < 0.6$ selection using hadronic system variables calculated with the Jaquet Blondel method [12].

Previous DIS studies [1, 2] included a further cut to remove events with little forward energy flow by requiring that the total summed energy deposited in the polar region $4^\circ < \theta < 15^\circ$ to be greater than 0.5 GeV. The discovery of diffractive events with a hard scale was a surprise and early DIS Monte–Carlos were incapable of their generation. The cut was designed to remove these events and defines the DIS event selection.

The diffractive event selection, DIFF, requires the absence of hadronic activity in the forward region. There must be no signal above noise levels in the FMD and PRT detectors. The most forward hadronic energy cluster with $E > 400$ MeV must be at $\eta < 3.3$. Non-diffractive contributions are further suppressed by explicitly requiring $x_{I\!P} < 0.05$. Contributions from light vector meson production are excluded by requiring $3.0 < M_{\mathrm{x}} < 36$ GeV. These cuts impose the approximate restrictions $M_Y \leq 1.6$ GeV and $|t| \leq 1$ GeV on the reconstructed events.

Following all the selection procedures $\sim 10^5$ events satisfy the DIS selection and $\sim 10^4$ events satisfy the DIFF selection.

In addition to these event selections there are also cuts made to reject badly measured tracks. Any tracks in the central chambers with transverse momenta below 150 MeV and those in the forward track detectors with momentum below 500 MeV are removed. We also remove tracks failing minimum requirements on the number of hits and the quality of the track fit. In order to determine the primary multiplicity, cuts are also made to exclude tracks not originating from the interaction vertex. There remains a small excess contribution due to the decays of short-lived strange particles.

To correct for this excess and for acceptance losses, we utilise the DJANGO [13] Monte-Carlo event generator for the DIS event selection. This combines a leading order (LO) perturbative QCD matrix element calculation and the colour dipole model with a calculation of QED radiative effects. For the DIFF selection we use the RAPGAP [14] Monte-Carlo. This combines a model of diffraction as deep-inelastic scattering of a virtual photon off a pomeron or reggeon coupled to the initial-state proton with the LEPTO [15] Monte-Carlo.

Radiative effects remaining after our event selections have been corrected for by comparing the results of Monte Carlo calculations with and without the inclusion of QED radiative effects. The detector response is simulated using a program based on the GEANT [16] package and the simulated events are reconstructed and selected using exactly the same analysis chain as with real data. No particle identification is used in this analysis. We adopt the procedure throughout of assuming that each charged particle is a pion and then using the same Monte Carlo simulation procedure to correct for the $\sim 12\%$ charged kaon and $\sim 5\%$ proton content.

A large source of systematic error for this analysis originates in possible calibration errors of $\pm 1\%$ for the SPACAL electromagnetic calorimeter energy scale since this directly affects the accuracy of Lorentz boosts and translates into uncertainties on the number of tracks in the area of interest of $\pm 7\%$ throughout (in a highly correlated fashion). The systematic error in the Monte-Carlo derived acceptance correction functions has been estimated using two different generators [13, 15] and is $\pm 7\%$.

The full experimental details of how the corrected distributions of this analysis are obtained from the data may be found in reference [17].

4 Rapidity Spectra

The rapidity, Y, for a given hadron is defined as

$$Y = \frac{1}{2} \ln \left(\frac{E + p_z}{E - p_z} \right) \tag{4}$$

where p_z is the longitudinal momentum of each track and the energy, E, is calculated assuming each charged hadron has the mass of a charged pion ,m_π. Corrections are made using Monte-Carlo to take admixture of other particles into account.

For both event selections the total width of the Y distribution, the longitudinal phase space, scales with energy and is typically given by $2\ln(W/m_\pi)$, while the width of the current hemisphere of the Breit frame is given by $\ln(Q/m_\pi)$. For diffractive events the expected width of the observed $\gamma^* I\!\!P$ system is given by $2\ln(M_{\mathrm{x}}/m_\pi)$ with a large rapidity gap separating it from the (unobserved) M_Y system in the extreme forward region.

Figure 1(a) shows the event normalised rapidity distribution for DIS and DIFF event selections for all Q^2. Compared with DIS, diffractive events have a higher multiplicity in the current region. This is discussed in detail in section 6. By definition, the multiplicity of diffractive events must approach zero at the beginning of the rapidity gap as is clearly seen in the DIFF selection. The distribution for the DIS selection, which has no requirement for a rapidity gap, shows a plateau in the target region which has been investigated elsewhere [2].

In [18] the H1 collaboration interpreted the measurement of the diffractive structure function, $F_2^{D(3)}$, in terms of a resolved pomeron model incorporating a leading diffractive exchange and a subleading reggeon contribution. Three different parameterisations were presented, a quark dominated parameterisation (fit 1) and two gluon dominated parton distributions, a 'flat gluon' (fit 2) and a 'peaked gluon (fit 3). Figure 1 shows that (the generally preferred) fit 2 gives a good description of the DIFF rapidity distribution.

In [19] a parameterisation has been made of the diffractive DIS cross section, the main feature of which is the decomposition of the β spectrum into three contributions: $q\bar{q}g$ production

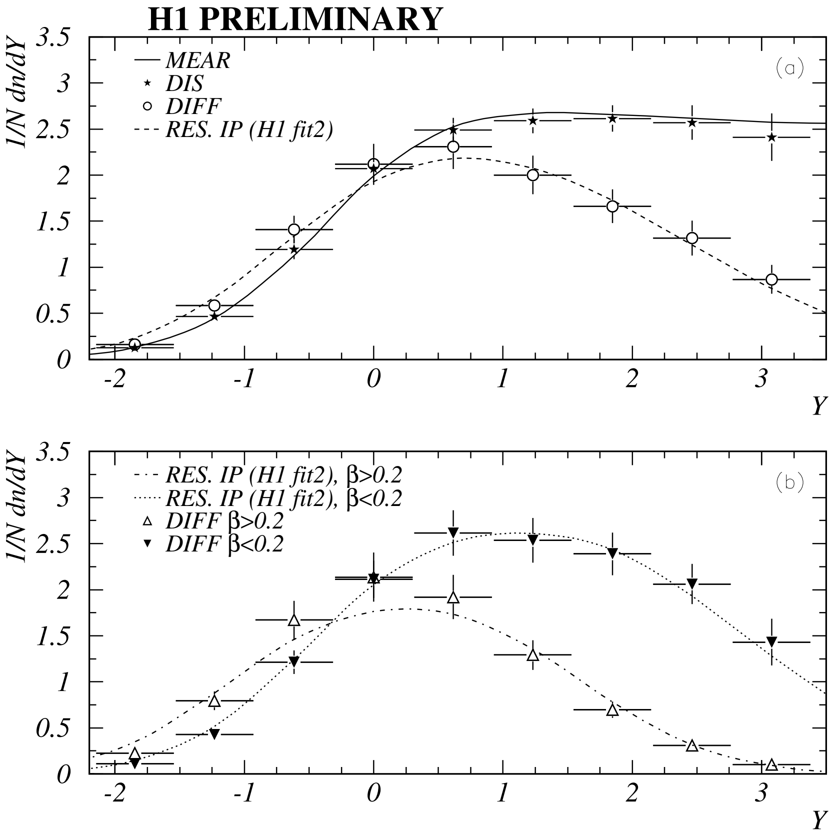

Figure 1: Rapidity distribution in the Breit frame of reference. (a) Comparison of DIS and DIFF. (b) Comparison of $\beta < 0.2$ and $\beta > 0.2$ for DIFF selected events. The data is compared with MEAR Monte-Carlo for DIS events and with RAPGAP using the resolved $I\!P$ model and the fit 2 parameterisation from H1 [18].

(dominating at low β ($\beta <\sim 0.2$)) and transverse and longitudinal $q\overline{q}$ production (dominating at medium and high β). This motivates the subdivision of the DIFF selection into two different β regions. Figure 1(b) shows that for $\beta > 0.2$ the rapidity distribution is symmetric about the Breit frame origin, consistent with the back-to-back emission of a pair of quarks in either hemisphere. The selection $\beta < 0.2$ gives a broader and more asymmetric distribution extending further into the target hemisphere of the Breit frame. This is consistent with a $q\overline{q}g$ system as claimed in [19]. It also results in higher total multiplicity which is also expected kinematically since lower β values correspond to higher values of M_x.

It is noticeable that the β dependence seen figure 1(b) is described by the resolved pomeron model. Other models of diffraction are compared in Figures 2 and 3 and show that fit2 and fit 3 cannot be differentiated and provide the best description of the data. Fit 1 clearly does not describe the data and shows that the rapidity distribution is sensitive to different models of diffraction.

Diffractive DIS can be treated (in the proton rest frame) by considering the $q\overline{q}$ and $q\overline{q}g$ photon fluctuations as colour dipoles [19]. The saturation model by Golec-Biernat and Wusthoff [21] uses the colour dipole approach, with an ansatz for the dipole cross section which interpolates between the perturbative and non-perturbative regimes of the $\gamma^* p$ cross section. The model does not describe the data as well as fits 2 and 3 of the resolved pomeron model, predicting a lower multiplicity in the central region.

In the soft colour interaction model (SCI), diffraction occurs through soft colour rearrangements between the outgoing partons The original SCI model [22] used only one free parameter, the universal colour rearrangement probability, fixed by a fit to $\mathrm{F}_2^{D(3)}$. A recent refinement to the model [23] has been made by making the colour rearrangement probability proportional to the normalised difference in the generalised area of the string configurations before and after the rearrangement.

SCI as implemented in LEPTO both in the original and refined forms together with a version of LEPTO without SCI are compared with the data in figure 3. The new versions of SCI improves the description of the rapidity spectra for DIS in the target region compared to the old version but still the version of LEPTO without SCI gives a better description. Despite the significant changes to the rapidity spectra for DIS the diffractive distributions show very little effect of these changes. SCI describes the rapidity spectra at high β but underestimates the multiplicity in the target region at low β.

All the models discussed are able to describe at least qualitatively the differences between high and low β indicating that they are mainly resulting from phase space restrictions which are due to the correlation between β and M_x.

5 Fragmentation Function

The ratio of the momentum of any particular charged hadron to the energy scale ($Q/2$) of the current hemisphere of the Breit frame is $x_p = p^{\pm}_{hadron}/(Q/2)$. It has been shown to be directly comparable to $x_p = p^{\pm}_{hadron}/(E^*/2)$ [1] for one hemisphere of an e^+e^- experiment where $\sqrt{s_{ee}} = E^* = Q$. The event normalised charged track density,

$$D^{\pm}(x_p) = \left(\frac{1}{N}\right) \times dn^{\pm}_{tracks}/dx_p \qquad (5)$$

is called the fragmentation function which characterises the complete process of final state parton shower development and non-perturbative hadronisation. The fragmentation function

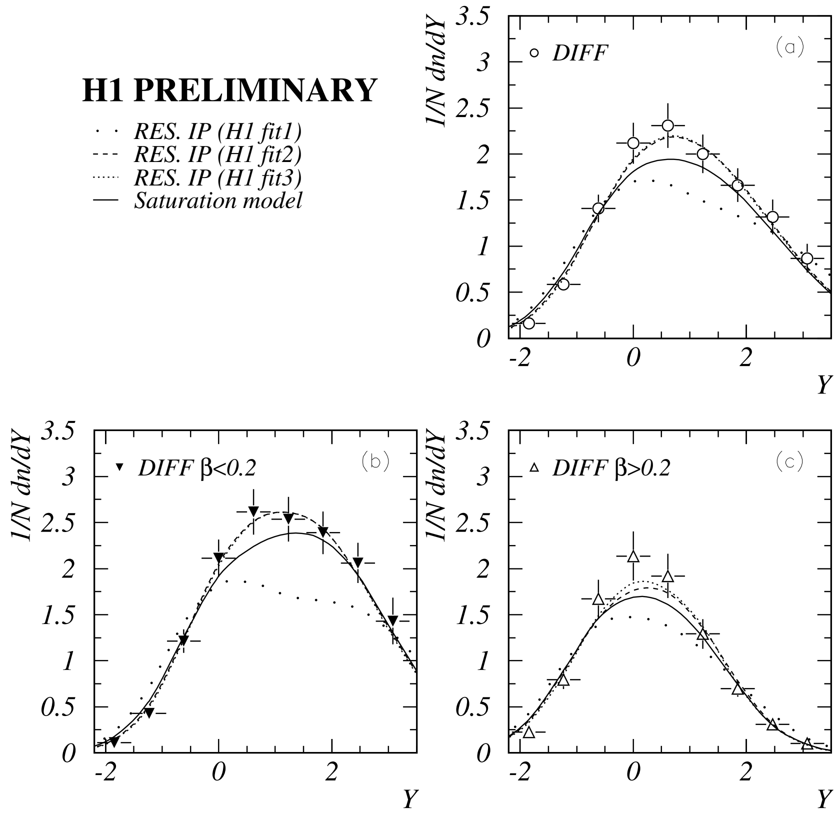

Figure 2: Comparison of rapidity distributions with predictions from a resolved pomeron model using three different parameterisations from H1[18], and the saturation model [21].

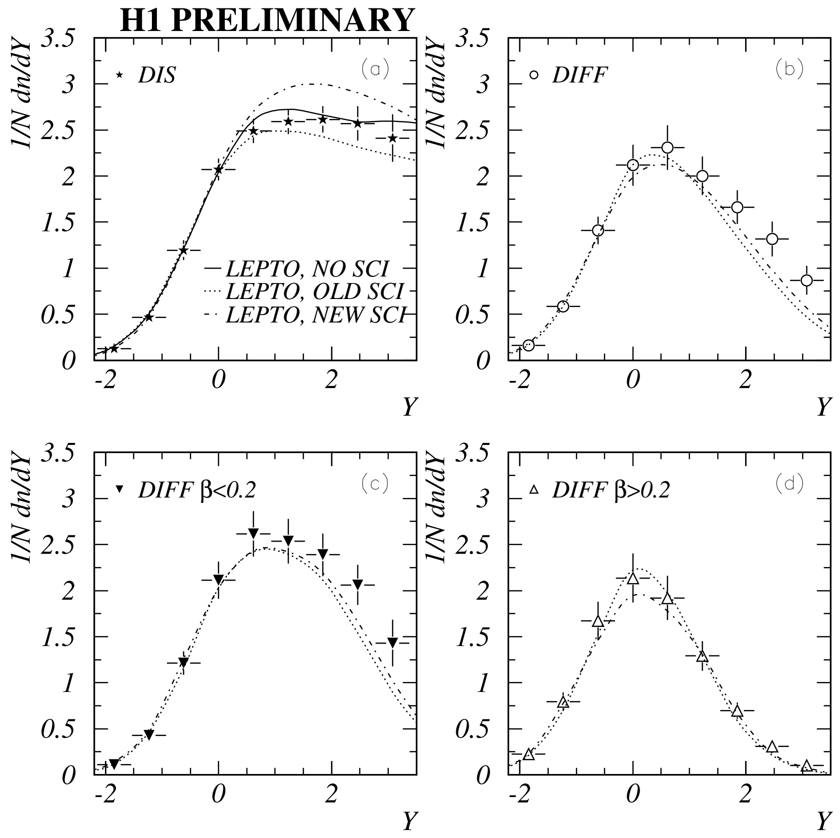

Figure 3: Comparison of rapidity distributions with predictions from the LEPTO Monte-Carlo with different implementations of Soft Colour Interactions (SCI).

may be redefined to

$$D^{\pm}(\xi) = \left(\frac{1}{N}\right) \times dn^{\pm}_{tracks}/d\xi \tag{6}$$

by change of variable to $\xi = \ln\left(\frac{1}{x_p}\right)$, which is used to expand the low momentum region.

The Modified Leading Log Approximation (MLLA) [24] coupled together with Local Parton Hadron Duality (LPHD) predicts that in the region of the peak of the hadronic ξ distribution, the shape is approximately Gaussian. The MLLA also gives a prediction for the energy behaviour of the peak position and width of this Gaussian (the first and second moments of the fragmentation function respectively);

$$\xi_{peak} = 0.5U + c_2\sqrt{U} + O(1) \tag{7}$$

$$\xi_{width} = \sqrt{\frac{U^{3/2}}{2c_1}}. \tag{8}$$

Here $U = \ln(Q/\Lambda_{eff})$, where Λ_{eff} is an effective scale parameter, c_1 and c_2 are constants dependent on the number of excited flavours and colours in QCD, and $O(1)$ is a slowly varying function of energy containing all QCD diagrams beyond leading order. This term is assumed to be constant in this analysis.

Figure 4 summarises the energy evolution of the fragmentation function. The solid (dashed) line is the simultaneous fit to the peak position and width of the MLLA parameterisation for the DIS (DIFF) data selection which yields a result of $\Lambda_{eff} = 0.21 \pm 0.04$ (0.19 ± 0.03) and $O(1) = -0.42 \pm 0.12$ (-0.49 ± 0.12).

Both DIS and DIFF distributions and parameters are compatible with each other, thus lending further support to the concept of quark fragmentation universality.

6 Average Charged Multiplicity

The area under the fragmentation function is the averaged charged multiplicity, $<n>$, also known as the zeroth moment of the fragmentation function. Figure 5 compares the average charged multiplicity in the current region between DIS and DIFF and the data is compared with MEAR Monte-Carlo for DIS events and with RAPGAP using the resolved $I\!P$ model and the fit 2 parameterisation from H1 [18]. In figure 6 the diffractive data is compared with predictions from the saturation model. The DIFF selection is split into high and low β samples and shown together with a parameterisation [25] of e^+e^- results for a single hemisphere, where contributions from K^0 and Λ decays have been subtracted, to be comparable with this data.

In [1], the observation of a significant shortfall of $<n>$ for DIS compared to e^+e^- was explained by LO QCD processes present in ep but absent in e^+e^- interactions. Such higher order QCD processes lead to a depopulation of tracks in the current region (or even an empty current region). This effect is also observed for the low β DIFF selection which is expected to be dominated by $q\overline{q}g$ production. The high β DIFF selection which is expected to be dominated by $q\overline{q}$ production, compares well with the e^+e^- parameterisation and has significantly fewer events with an empty current region[2]. For $12 < Q^2 < 15$ $(60 < Q^2 < 80)$ GeV^2, 28% (10%) of events in the DIS selection have an empty current region, compared with 22% (7%) in the DIFF sample at low β and 8% (3%) at high β. As with the rapidity spectra both the resolved

[2]Note that for $\mathrm{M_x} < Q$ $(\beta > 0.5)$ it is kinematically forbidden to have an empty current region.

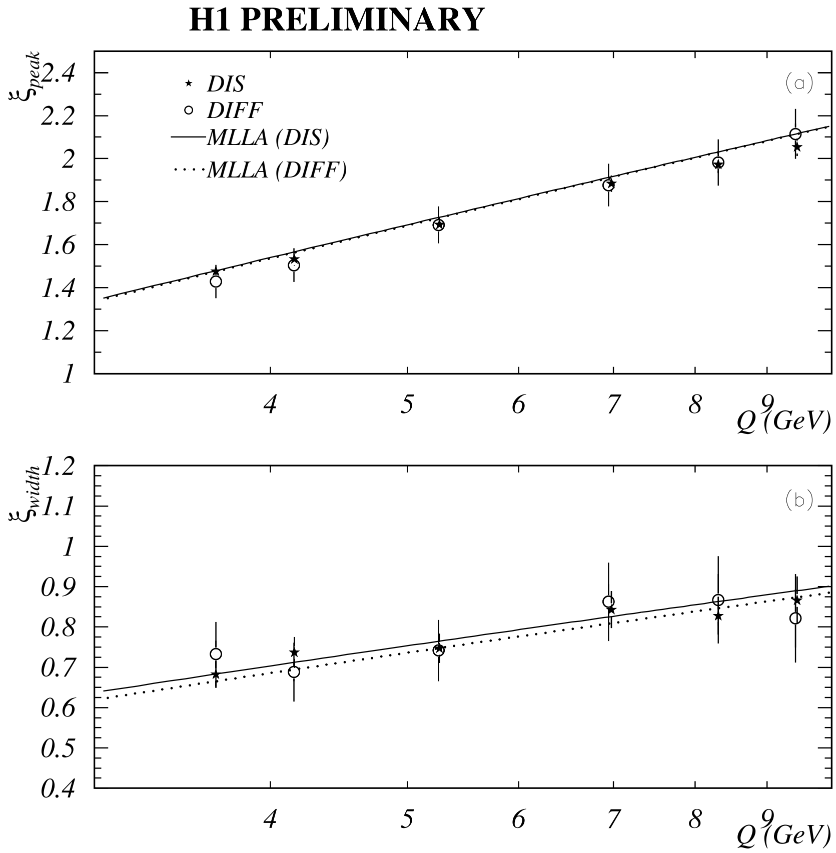

Figure 4: The energy evolution of the (a) peak position and (b) width of the fragmentation function for both DIS and DIFF selections. The solid (dashed) line is the simultaneous fit of the MLLA parameterisation to the DIS (DIFF) data.

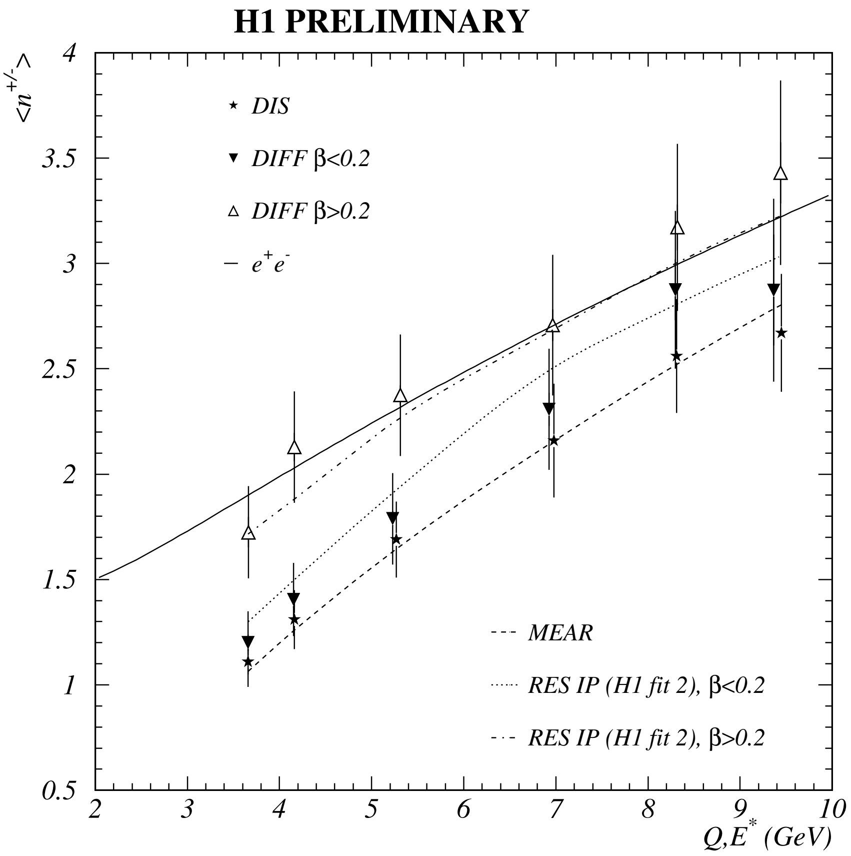

Figure 5: The average charged multiplicities as a function of the energy scale Q. The error is dominated by a correlated systematic error of about $\sim 7\%$ associated with the energy uncertainty of the scattered electron in the SpaCal. The solid curve is a fit to many e^+e^- results as a function of the centre of mass energy $E^*(E^* = Q)$, the dashed line a prediction for the MEAR Monte-Carlo for DIS events and the dotted and dashed-dotted lines comes from RAPGAP using the resolved $I\!\!P$ model and the fit 2 parameterisation from H1 [18].

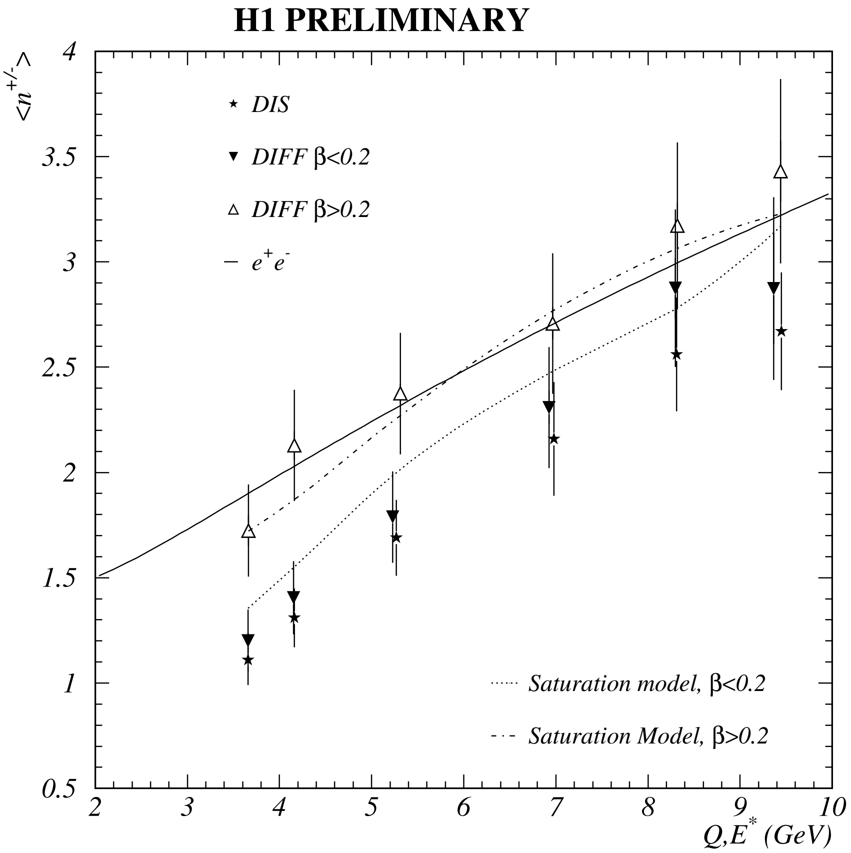

Figure 6: The average charged multiplicities as a function of the energy scale Q. The data is compared with a prediction of the saturation model.

pomeron model (H1 fit 2) and the saturation model are able to describe the β dependence and the Q^2 evolution of the average charged multiplicity seen in the data.

7 Conclusions

The universality of quark fragmentation has been supported by comparing spectra for quarks originating from the pomeron with those from quarks from the proton and from quarks produced from the vacuum in e^+e^- annihilation experiments.

The β dependence of diffractive DIS data is consistent with the expectation for final states of $q\bar{q}g$ at low β and for $q\bar{q}$ at high β but is also reproduced in models where there is no explicit modeling of these final state configurations, strongly suggesting that these effects are a result of restricting the phase space that is implicit in making a selection of β.

Acknowledgments

We are grateful to the HERA machine group whose outstanding efforts have made and continue to make this experiment possible. We thank the engineers and technicians for their work in constructing and now maintaining the H1 detector, our funding agencies for financial support, the DESY technical staff for continual assistance, and the DESY directorate for the hospitality which they extend to the non–DESY members of the collaboration.

References

[1] H1 Collaboration, S. Aid et al., Nucl.Phys. B445, 3 (1995).
H1 Collaboration, C. Adloff et al., Nucl. Phys. B504, 3 (1997).

[2] H1 Collaboration, C. Adloff et al., 1998 ICHEP98: 29th Int. Conf. on High Energy Physics (Vancover, Canada) July 1998 p 531.

[3] ZEUS Collaboration, M. Derrick et al., Z. Phys. C67, 93 (1995).
ZEUS Collaboration., M. Derrick et al., Phys. Lett. B414, 428 (1997).

[4] ZEUS Collaboration, J. Breitweg et al., Eur. Phys. J. C11, 251 (1999).

[5] R.P. Feynman, 'Photon-Hadron Interactions', Benjamin, N.Y. (1972).

[6] H1 Collaboration. Eur. Phys. J. C5, 439-452 (1998)
H1 Collaboration. C. Adloff et al., Phys. Lett. B428, 206-220 (1998)

[7] H1 Collaboration, I. Abt et al., DESY preprint 93-103 (1993), Nucl. Instrum. Methods A386, 310 (1997) (Vol 1) and ibid. p348 (Vol 2).

[8] J. Burger et al., Nucl. Instrum. Methods A279, 217 (1989).

[9] H1 FTD group, S.Burke et al., Nucl. Instrum. Methods A373, 227 (1996)

[10] H1 calorimeter group, B.Andrieu et al., Nucl. Instrum. Methods A336, 460 (1993)

[11] H1 SPACAL group, R.D. Appuhn et al., DESY preprint 96-171 (1996), submitted to Nucl. Instr. and Meth.

[12] Proceedings of the study of an ep facility for Europe, Ed. U. Amaldi, DESY 79/48 (1979) p391-4.

[13] G.A. Schuler and H. Spiesberger, Proceedings of the Workshop: Physics at HERA, vol.~3 eds. W. Buchmuller, G. Ingelman, DESY (1992) 1419. We use version 6.2 with QED radiation simulated with HERACLES 4.4 when correcting data. QCD radiation is simulated by the colour dipole model (ARIADNE 4.08) and hadronisation with the LUND string model in JETSET 7.4. We use MRSH parton density parameterisations.

[14] H. Jong, Comp. Phys. Comm. 86 (1995) 147.

[15] LEPTO 6.5 Generator with GRV parton density functions ; G.Ingelman, Proceedings of the Workshop: Physics at HERA, vol. 3 eds. W.Buchmuller, G.Ingeman, DESY (1991) 1366.

[16] R. Brun et al., GEANT3 User's guide, CERN-DD/EE 84-1, Geneva (1987).

[17] D.P. Traynor, in litt. University of London thesis; K.T. Donovan, University of London thesis (1998) RAL-TH-1998-017.

[18] H1 Collaboration, C. Adloff et al., Z. Phys. C76, 613 (1997)

[19] J. Bartels et al. Eur. Phys. J C7, 443 (1999)

[20] H1 Collaboration, C. Adloff et al., Eur. Phys. J. C5, 439 (1998)

[21] K. Golec-Biernat, M. Wusthoff, Phys. Rev. D59, 014017 (1999), K. Golec-Biernat, M. Wusthoff, Phys. Rev. D60, 114023 (1999)

[22] A. Edin, G. Ingelman, J. Rathsman, Phys. Lett. B366, 371 (1996). A. Edin, G. Ingelman, J. Rathsman, Z. Phys. C75, 57 (1997)

[23] J. Rathsman, Phys. Lett. B452, 364 (1999)

[24] Yu.L. Dokshitzer, V.A. Khoze, A.H. Mueller and S.I. Troyan, "Basics of Perturbative QCD" Editions Frontieres.

[25] OPAL Collaboration, P.D. Acton et al., Z. Phys. C 53, 539 (1992)